4.4. Anti-tumor activity and the distribution of NK012 and CPT-11 in SBC-3/Neo or SBC-3/VEGF tumors

In order to determine whether the potent antitumor effect of NK012 is enhanced in the tumors with high vascularity, we used vascular endothelial growth factor-secreting cells SBC-3/VEGF. There was no significant difference in the *in vitro* cytotoxic activity of each drug between SBC-3/Neo and SBC-3/VEGF (Fig. 14A). Gross findings of SBC-3/VEGF tumors are reddish as compared with SBC-3/Neo tumors (Fig. 14B). Deviating from the ordinary experimental tumor model, tumors were allowed to grow until they became massive in size, around 1.5 cm (Fig. 14C), and then the treatment was initiated. NK012 at doses of 15 and 30 mg/kg showed potent anti-tumor activity against bulky SBC-3/Neo tumors (1533.1 ± 1204.7 mm^3) as compared with CPT-11 (Fig. 14C). Striking antitumor activity was observed in mice treated with NK012 (Fig. 14C) when we compared the antitumor activity of NK012 with CPT-11 using SBC-3/VEGF cells. SBC-3/VEGF bulky masses (1620.7 ± 834.0 mm^3) disappeared in all mice, although relapse 3 months after treatment was noted in one mouse treated with NK012 20 mg/kg. On the other hand, SBC-3/VEGF were not eradicated and rapidly regrew after a partial response in mice treated with CPT-11. Approximate 10% body weight loss was observed in mice treated with NK012 20 mg/kg, but no significant difference was observed in comparison with mice treated with CPT-11 30 mg/kg.

We then examined the distribution of free SN-38 in the SBC-3/Neo and SBC-3/VEGF masses after administration of NK012 and CPT-11. In the case of CPT-11 administration, the concentrations at 1 and 6 h after the administration were less than 100 ng/g both in the SBC-3/Neo and SBC-3/VEGF tumors, and were almost negligible at 24 h in both tumors (Fig. 15A). There was no significant difference in the concentration between the SBC-3/Neo and SBC-3/VEGF tumors. On the other hand, in the case of NK012 administration, free SN-38 was detectable in the tumors even at 72 h after the administration. The concentrations of free SN-38 were higher in the SBC-3/VEGF tumors than those in the SBC-3/Neo tumors at any time point during the period of observation (significant at 1, 6, 24 h. $^*P<0.05$) (Fig. 15A).

4.5. Tissue distribution of SN-38 after administration of NK012 and CPT-11

We examined the concentration-time profile of free SN-38 in various tissues after *i.v.* administration of NK012 and CPT-11. All organs measured exhibited the highest concentration of SN-38 at 1 h after administration in mice given CPT-11 (Fig. 15B). On the other hand, mice given NK012 exhibited prolonged distribution in the liver and spleen (Fig. 15B). In a similar manner to other micellar drugs [39,53], NK012 demonstrated relatively higher accumulation in organs of the reticuloendothelial system. In the lung, kidney and small intestine, the highest concentration of free SN-38 was achieved at 1 h after injection of NK012 and the concentration was almost negligible at 24 h. Although the concentrations of free SN-38 in the small intestine were relatively high at 1 h after administration of NK012 and CPT-11, those rapidly decreased. Interestingly, there was no significant difference in the kinetic character of free SN-38 in the small intestine between mice treated with NK012 and CPT-11.

4.6. Synergistic antitumor activity of the NK012 combined with 5-fluorouracil

In two phase III trials, the addition of CPT-11 to bolus or infusional 5FU/LV regimens clearly yielded greater efficacy than treatment with 5FU/LV alone, with a doubling of the tumor response rate and prolongation of the median survival time by 2–3 months [54,55].

We demonstrated that the novel SN-38-incorporating polymeric micelles, NK012, exerted superior antitumor activity and less toxicity as compared to CPT-11[53]. Therefore, we speculated that the use of NK012 in place of CPT-11 in combination with 5FU may also yield superior results.

4.6.1. Comparison of the antitumor effect of combined NK012/5FU and CPT-11/5FU

The therapeutic effect of CPT-11/5FUwas apparently inferior to that of NK012/5FU or even NK012 alone at the MTD (Fig. 13). A more potent antitumor effect, namely 100% CR rate, was obtained in the NK012 alone and NK012/5FU groups, as compared with the 0% CR rate in the CPT-11/5FU [57].

4.6.2. Specificity of cell cycle perturbation

We studied the difference in the effects between NK012 and CPT-11 on the cell cycle. The data indicate that both NK012 and CPT-11 had a tendency to accumulate the cells in the S phase, although the effect of NK012 was stronger and maintained for a more prolonged period than that of CPT-11. The histograms show aneuploidy of the tumor and that administration of NK012 or CPT-11 caused apoptosis of a proportion of the tumor cells [57].

4.7. Present situation of a clinical study of NK012

A phase 1 study of NK012 is now under way in the National Cancer Center, Tokyo and Kashiwa in patients with advanced solid tumors. NK012 is infused intravenously over 60 min every 21 days until disease progression or unacceptable toxicity occurs.

5. Conclusion

A quarter of a century has passed since the EPR effect was discovered. Now the phrase EPR has become a fundamental principle in the field of DDS. Until recently, the EPR had not been recognized in the field of oncology. However, many oncologists have now become acquainted with it, since some drugs such as doxil, abraxane, and several PEGylated proteinacious agents formulated based on the EPR have been approved in the field of oncology. Micelle carrier systems described in this chapter are obviously categorized as DDS based on the EPR. I believe that some anticancer agents incorporating micelle nanoparticles may be approved for clinical use soon.

Our next task is to develop DDS utilizing the EPR effect, which can accumulate selectively in solid tumors but also allow distribution of the delivered bullets (anticancer agents) through the entire mass of the solid tumor tissue.

References

[1] Y. Matsumura, H. Maeda, A new concept for macromolecular therapeutics in cancer chemotherapy: mechanism of tumoritropic accumulation of proteins and the antitumor agent SMANCS, Cancer Res. 46 (1986) 6387–6392.

[2] K. Kataoka, G.S. Kwon, M. Yokoyama, T. Okano, Y. Sakurai, Block copolymer micelles as vehicles for drug delivery, J. Control. Release 24 (1993) 119–132.

[3] M. Yokoyama, M. Miyauchi, N. Yamada, T. Okano, Y. Sakurai, K. Kataoka, S. Inoue, Polymer micelles as novel drug carrier: adriamycin-conjugted poly(ethylene glycol)-poly(aspartic acid) block copolymer, J. Control. Release 11 (1990) 269–278.

[4] M. Yokoyama, T. Okano, Y. Sakurai, H. Ekimoto, C. Shibazaki, K. Kataoka, Toxicity and antitumor activity against solid tumors of micelle-forming polymeric anticancer drug and its extremely long circulation in blood, Cancer Res. 51 (1991) 3229–3236.

[5] D. Khayat, E.C. Antoine, D. Coeffic, Taxol in the management of cancers of the breast and the ovary, Cancer Invest. 18 (2000) 242–260.

[6] D.N. Carney, Chemotherapy in the management of patients with inoperable non-small cell lung cancer, Semin. Oncol. 23 (1996) 71–75.

[7] R.B. Weiss, R.C. Donehower, P.H. Wiernik, T. Ohnuma, R.J. Gralla, D.L. Trump, J.R. Baker Jr, D.A. Van Echo, D.D. Von Hoff, B. Leyland-Jones, Hypersensitivity reactions from taxol, J. Clin. Oncol. 8 (1990) 1263–1268.

[8] E.K. Rowinsky, R.C. Donehower, Paclitaxel (taxol), N. Engl. J. Med. 332 (1995) 1004–1014;
R. Savic, L. Luo, A. Eisenberg, D. Maysinger, Micellar nanocontainers distribute to defined cytoplasmic organelles, Science 300 (2003) 615–618.

[9] E.K. Rowinsky, V. Chaudhry, A.A. Forastiere, S.E. Sartorius, D.S. Ettinger, L.B. Grochow, B.G. Lubejko, D.R. Cornblath, R.C. Donehower, Phase I and pharmacologic study of paclitaxel and cisplatin with granulocyte colony-stimulating factor: neuromuscular toxicity is dose-limiting, J. Clin. Oncol. 11 (1993) 2010–2020.

[10] C. Wasserheit, A. Frazein, R. Oratz, J. Sorich, A. Downey, H. Hochster, A. Chachoua, J. Wernz, A. Zeleniuch-Jacquotte, R. Blum, J. Speyer, Phase II trial of paclitaxel and cisplatin in women with advanced breast cancer: an active regimen with limiting neurotoxicity, J. Clin. Oncol. 14 (1996) 1993–1999.

[11] M. Yokoyama, T. Okano, Y. Sakurai, H. Ekimoto, C. Shibazaki, K. Kataoka, Toxicity and antitumor activity against solid tumors of micelle-forming polymeric anticancer drug and its extremely long circulation in blood, Cancer Res. 51 (1991) 3229–3236.

[12] T. Hamaguchi, Y. Matsumura, M. Susuki, K. Shimizu, R. Goda, I. Nakamura, M. Nakatomi, K. Yokoyama, K. Kataoka, T. Kakizoe, NK105, a paclitaxel-incorporating micellar nanoparticle formulation, can extend in vivo antitumour activity and reduce the neurotoxicity of paclitaxel, Br. J. Cancer 92 (2005) 1240–1246.

[13] R.B. Tishler, C.R. Geard, E.J. Hall, P.B. Schiff, Taxol sensitizes human astrocytoma cells to radiation, Cancer Res. 52 (1992) 3495–3497.

[14] H. Choy, R.F. Devore 3rd, K.R. Hande, L.L. Porter, P. Rosenblatt, F. Yunus, L. Schlabach, C. Smith, Y. Shyr, D.H. Johnson, A phase II study of paclitaxel, carboplatin, and hyperfractionated radiation therapy for locally advanced inoperable non-small-cell lung cancer (a Vanderbilt Cancer Center Affiliate Network Study), Int. J. Radiat. Oncol. Biol. Phys. 47 (2000) 931–937.

[15] M. Rodriguez, B.U. Sevin, J. Perras, H.N. Nguyen, C. Pham, A.J. Steren, O.R. Koechli, H.E. Averette, Paclitaxel: a radiation sensitizer of human cervical cancer cells, Gynecol. Oncol. 57 (1995) 165–169.

[16] B.L. Lokeshwar, S.M. Ferrell, N.L. Block, Enhancement of radiation response of prostatic carcinoma by taxol: therapeutic potential for late-stage malignancy, Anticancer Res. 15 (1995) 93–98.

[17] L. Milas, N.R. Hunter, K.A. Mason, B. Kurdoglu, L.J. Peters, Enhancement of tumor radioresponse of a murine mammary carcinoma by paclitaxel, Cancer Res. 54 (1994) 3506–3510.

[18] L. Milas, N.R. Hunter, K.A. Mason, C.G. Milross, Y. Saito, L.J. Peters, Role of reoxygenation in induction of enhancement of tumor radioresponse by paclitaxel, Cancer Res. 55 (1995) 3564–3568.

[19] A. Cividalli, G. Arcangeli, G. Cruciani, E. Livdi, E. Cordelli, D.T. Danesi, Enhancement of radiation response by paclitaxel in mice according to different treatment schedules, Int. J. Radiat. Oncol. Biol. Phys. 40 (1998) 1163–1170.

[20] R.B. Tishler, C.R. Geard, E.J. Hall, P.B. Schiff, Taxol sensitizes human astrocytoma cells to radiation, Cancer Res. 52 (1992) 3495–3497.

[21] A.G. Taghian, S.I. Assaad, A. Niemierko, I. Kuter, J. Younger, R. Schoenthaler, M. Roche, S.N. Powell, Risk of pneumonitis in breast cancer patients treated with radiation therapy and combination chemotherapy with paclitaxel, J. Natl. Cancer Inst. 93 (2001) 1806–1811.

[22] H. Choy, W. Akerley, H. Safran, S. Graziano, C. Chung, T. Williams, B. Cole, T. Kennedy, Multiinstitutional phase II trial of paclitaxel, carboplatin, and concurrent radiation therapy for locally advanced non-small-cell lung cancer, J. Clin. Oncol. 16 (1998) 3316–3322.

[23] J.E. Dowell, R. Sinard, D.A. Yardley, V. Aviles, M. Machtay, R.S. Weber, G.S. Weinstein, A.A. Chalian, D.P. Carbone, D.I. Rosenthal, Seven-week continuous-infusion paclitaxel concurrent with radiation therapy for locally advanced non-small cell lung and head and neck cancers, Semin. Radiat. Oncol. 9 (1999) 97–101.

[24] D.P. Penney, P. Rubin, Specific early fine structural changes in the lung irradiation, Int. J. Radiat. Oncol. Biol. Phys. 2 (1977) 1123–1132.

[25] P.A. Lind, L.B. Marks, P.H. Hardenbergh, R. Clough, M. Fan, D. Hollis, M.L. Hernando, D. Lucas, A. Piepgrass, L.R. Prosnitz, Technical factors associated with radiation pneumonitis after local +/− regional radiation therapy for breast cancer, Int. J. Radiat. Oncol. Biol. Phys. 52 (2002) 137–143.

[26] A.G. Taghian, S.I. Assaad, A. Niemierko, I. Kuter, J. Younger, R. Schoenthaler, M. Roche, S.N. Powell, Risk of pneumonitis in breast cancer patients treated with radiation therapy and combination chemotherapy with paclitaxel, J. Natl. Cancer. Inst. 93 (2001) 1806–1811.

[27] Y.M. Hanna, K.L. Baglan, J.S. Stromberg, F.A. Vicini, D. A Decker, Acute and subacute toxicity associated with concurrent adjuvant radiation therapy and paclitaxel in primary breast cancer therapy, Breast J. 8 (2002) 149–153.

[28] T. Negishi, F. Koizumi, H. Uchino, J. Kuroda, T. Kawaguchi, S. Naito, Y. Matsumura, NK105, a paclitaxel-incorporating micellar nanoparticle, is a more potent radiosensitising agent compared to free paclitaxel, Br. J. Cancer 95 (2006) 601–606.

[29] T. Hamaguchi, K. Kato, H. Yasui, C. Morizane, M. Ikeda, H. Uchino, K. Muro, Y. Yamada, T. Okusaka, K. Shirao, Y. Yamada, H. Nakahama, Y. Matsumura, A phase I and pharmacokinetic study of NK105, a paclitaxel-incorporating micellar nanoparticle formulation, Br. J. Cancer 97 (2007) 170–176.

[30] A. Horwich, D.T. Sleijfer, S.D. Fossa, S.B. Kaye, R.T. Oliver, M.H. Cullen, G.M. Mead, R. de Wit, P.H. de Mulder, D.P. Dearnaley, P.A. Cook, R.J. Sylvester, S.P. Stenning, Randomized trial of bleomycin, etoposide, and cisplatin compared with bleomycin, etoposide, and carboplatin in good-prognosis metastatic nonseminomatous germ cell cancer: a Multiinstitutional Medical Research Council/European Organization for Research and Treatment of Cancer Trial, J. Clin. Oncol. 15 (1997) 1844–1852.

[31] B.J. Roth, Chemotherapy for advanced bladder cancer, Semin. Oncol. 23 (1996) 633–644;
D. Screnci, M.J. McKeage, P. Galettis, T.W. Hambley, B.D. Palmer, B.C. Baguley, Relationships between hydrophobicity, reactivity, accumulation and peripheral nerve toxicity of a series of platinum drugs, Br. J. Cancer. 82 (2000) 966–972.

[32] V. Pinzani, F. Bressolle, I.J. Haug, M. Galtier, J.P. Blayac, P. Balmes, Cisplatin-induced renal toxicity and toxicity-modulating strategies: a review, Cancer Chemother. Pharmacol. 35 (1994) 1–9.

[33] M.J. Cleare, P.C. Hydes, B.W. Malerbi, D.M. Watkins, Anti-tumor platinum complexes: relationships between chemical properties and activity, Biochimie 60 (1978) 835–850.

[34] A. du Bois, H.J. Luck, W. Meier, H.P. Adams, V. Mobus, S. Costa, T. Bauknecht, B. Richter, M. Warm, W. Schroder, S. Olbricht, U. Nitz, C. Jackisch, G. Emons, U. Wagner, W. Kuhn, J. Pfisterer, A randomized clinical trial of cisplatin/paclitaxel versus carboplatin/paclitaxel as first-line treatment of ovarian cancer, J. Natl. Cancer Inst. 95 (2003) 1320–1329.

[35] J. Cassidy, J. Tabernero, C. Twelves, R. Brunet, C. Butts, T. Conroy, F. Debraud, A. Figer, J. Grossmann, N. Sawada, P. Schoffski, A. Sobrero, E. Van Cutsem, E. Diaz-Rubio, XELOX (capecitabine plus oxaliplatin): active first-line therapy for patients with metastatic colorectal cancer, J. Clin. Oncol. 22 (2004) 2084–2091.

[36] A. Horwich, D.T. Sleijfer, S.D. Fossa, S.B. Kaye, R.T. Oliver, M.H. Cullen, G.M. Mead, R. de Wit, P.H. de Mulder, D.P. Dearnaley, P.A. Cook, R.J. Sylvester, S.P. Stenning, Randomized trial of bleomycin, etoposide, and cisplatin compared with bleomycin, etoposide, and carboplatin in good-prognosis metastatic nonseminomatous germ cell cancer: a Multiinstitutional Medical Research Council/European Organization for Research and Treatment of Cancer Trial, J. Clin. Oncol. 15 (1997) 1844–1852.

[37] J. Bellmunt, A. Ribas, N. Eres, J. Albanell, C. Almanza, B. Bermejo, L.A. Sole, J. Baselga, Carboplatin-based versus cisplatin-based chemotherapy in the treatment of surgically incurable advanced bladder carcinoma, Cancer 80 (1997) 1966–1972.

[38] N. Nishiyama, S. Okazaki, H. Cabral, M. Miyamoto, Y. Kato, Y. Sugiyama, K. Nishio, Y. Matsumura, K. Kataoka, Novel cisplatin-incorporated polymeric micelles can eradicate solid tumors in mice, Cancer Res. 63 (2003) 8977–8983.

[39] H. Uchino, Y. Matsumura, T. Negishi, F. Koizumi, T. Hayashi, T. Honda, et al., Cisplatin-incorporating polymeric micelles (NC-6004) can reduce nephrotoxicity and neurotoxicity of cisplatin in rats, Br. J. Cancer 93 (2005) 678–687.

[40] L.H. Li, T.J. Fraser, E.J. Olin, B.K. Bhuyan, Action of camptothecin on mammalian cells in culture, Cancer Res. 32 (1972) 2643–2650.

[41] R.C. Gallo, J. Whang-Peng, R.H. Adamson, Studies on the antitumor activity, mechanism of action, and cell cycle effects of camptothecin, J. Natl. Cancer Inst. 46 (1971) 789–795.

[42] J.A. Gottlieb, A.M. Guarino, J.B. Call, V.T. Oliverio, J.B. Block, Preliminary pharmacologic and clinical evaluation of camptothecin sodium (NSC-100880), Cancer Chemother. Rep. 54 (1970) 461–470.

[43] F.M. Muggia, P.J. Creaven, H.H. Hansen, M.H. Cohen, O.S. Selawry, Phase I clinical trial of weekly and daily treatment with camptothecin (NSC-100880): correlation with preclinical studies, Cancer Chemother. Rep. 56 (1972) 515–521.

[44] D. Cunningham, S. Pyrhonen, R.D. James, C.J. Punt, T.F. Hickish, R. Heikkila, et al., Randomised trial of irinotecan plus supportive care versus supportive care alone after fluorouracil failure for patients with metastatic colorectal cancer, Lancet 352 (1998) 1413–1418.

[45] L.B. Saltz, J.V. Cox, C. Blanke, L.S. Rosen, L. Fehrenbacher, M.J. Moore, et al., Irinotecan plus fluorouracil and leucovorin for metastatic colorectal cancer. Irinotecan Study Group, N. Engl. J. Med. 343 (2000) 905–914.

[46] K. Noda, Y. Nishiwaki, M. Kawahara, S. Negoro, T. Sugiura, A. Yokoyama, et al., Irinotecan plus cisplatin compared with etoposide plus cisplatin for extensive small-cell lung cancer, N. Engl. J. Med. 346 (2002) 85–91.

[47] S. Negoro, N. Masuda, Y. Takada, T. Sugiura, S. Kudoh, N. Katakami, et al., CPT-11 Lung Cancer Study Group West. Randomised phase III trial of irinotecan combined with cisplatin for advanced non-small-cell lung cancer, Br. J. Cancer 88 (2003) 335–341.

[48] D.C. Bodurka, C. Levenback, J.K. Wolf, J. Gano, J.T. Wharton, J.J. Kavanagh, et al., Phase II trial of irinotecan in patients with metastatic epithelial ovarian cancer or peritoneal cancer, J. Clin. Oncol. 21 (2003) 291–297.

[49] C.H. Takimoto, S.G. Arbuck, Topoisomerase I targeting agents: the camptothecins, in: B.A. Chabner, DL Lango (Eds.), Cancer Chemotherapy and Biotherapy: Principal and Practice, 3rd ed, Lippincott Williams & Wilkins, Philadelphia (PA), 2001, pp. 579–646.

[50] J.G. Slatter, L.J. Schaaf, J.P. Sams, K.L. Feenstra, M.G. Johnson, P.A. Bombardt, et al., Pharmacokinetics, metabolism, and excretion of irinotecan (CPT-11) following I.V. infusion of [(14)C]CPT-11 in cancer patients, Drug Metab. Dispos. 28 (2000) 423–433.

[51] M.L. Rothenberg, J.G. Kuhn, H.A. Burris 3rd, J. Nelson, J.R. Eckardt, M. Tristan-Morales, et al., Phase I and pharmacokinetic trial of weekly CPT-11, J. Clin. Oncol. 11 (1993) 2194–2204.

[52] S. Guichard, C. Terret, I. Hennebelle, I. Lochon, P. Chevreau, E. Fretigny, et al., CPT-11 converting carboxylesterase and topoisomerase activities in tumor and normal colon and liver tissues, Br. J. Cancer 80 (1999) 364–370.

[53] M. Yokoyama, T. Okano, Y. Sakurai, H. Ekimoto, C. Shibazaki, K. Kataoka, Toxicity and antitumor activity against solid tumors of micelle-forming polymeric anticancer drug and its extremely long circulation in blood, Cancer Res. 51 (1991) 3229–3236.

[54] L.B. Saltz, J.Y. Douillard, N. Pirotta, et al., Irinotecan plus fluorouracil/leucovorin for metastatic colorectal cancer: a new survival standard, Oncologist 6 (2001) 81–91.

[55] J.Y. Douillard, D. Cunningham, A.D. Roth, et al., Irinotecan combined with fluorouracil compared with fluorouracil alone as first-line treatment for metastatic colorectal cancer: a multicentre randomised trial, Lancet 355 (2000) 1041–1047.

[56] F. Koizumi, M. Kitagawa, T. Negishi, et al., Novel SN-38-incorporating polymeric micelles, NK012, eradicate vascular endothelial growth factor-secreting bulky tumors, Cancer Res. 66 (2006) 10048–10056.

[57] T. Eguchi Nakajima, M. Yasunaga, Y. Kano, K. Shirao, Y. Shimada, Y. Matsumura, Synergistic antitumour activity of the novel SN-38-incorporating polymeric micelles, NK012, combined with 5-fluorouracil in a mouse model of colorectal cancer, as compared with that of irinotecan plus 5-fluorouracil, Int. J. Cancer. 122 (2008) 2148–2153.

Pathology International 2008; **58**: 407–414 doi:10.1111/j.1440-1827.2008.02245.x

Original Article

Novel recombinant congenic mouse strain developing arthritis with enthesopathy

Shiro Mori,[1] Naoko Tanda,[1] Mitsuko R. Ito,[2] Hisashi Oishi,[2] Takahito Tsubaki,[2] Hiroaki Komori,[2] Ming-Cai Zhang,[3] Masao Ono,[3] Masahiko Nishimura[4] and Masato Nose[2]

[1]*Tohoku University Graduate School of Dentistry,* [3]*Tohoku University Graduate School of Medicine, Sendai,* [2]*Ehime University Graduate School of Medicine, Ehime and* [4]*Nagoya University Graduate School of Medicine, Nagoya, Japan*

Based on the hypothesis that the complex pathological and immunological manifestations of rheumatoid arthritis (RA) and the related diseases are under the control of multiple gene loci with allelic polymorphism, a recombinant congenic mouse strain was prepared between an MRL/Mp-*lpr/lpr* (MRL/lpr) strain, which develops arthritis resembling RA, and a non-arthritic strain C3H/HeJ-*lpr/lpr* (C3H/lpr). In MRL/lpr × (MRL/lpr × C3H/lpr) F1 mice, the mice developing severe arthritis were selected based on joint swelling to further continue intercrosses, and then an McH-*lpr/lpr*-RA1 (McH/lpr-RA1) strain was established and its histopathological phenotypes of joints and autoimmune traits were analyzed. Arthritis in McH/lpr-RA1 mice developed at a higher incidence by 20 weeks of age, compared with that in the MRL/lpr mice, who had severe synovitis (ankle, 60.3%; knee, 65.1%), and also fibrous and fibrocartilaginous lesions of articular ligamenta resembling enthesopathy (ankle, 79.4%; knee, 38.1%), resulting in ankylosis. The lymphoproliferative disorder was less, and serum levels of IgG and IgG autoantibodies including anti-dsDNA and rheumatoid factor were lower than those of both MRL/lpr and C3H/lpr strains. McH/lpr-RA1 mice may provide a new insight into the study of RA regarding the common genomic spectrum of seronegative RA and enthesopathy.

Key words: ankylosis, enthesitis, MRL/ lpr, rheumatoid arthritis, rheumatoid factor, seronegative, synovitis

Rheumatoid arthritis and the related diseases such as spondyloarthropathy and juvenile idiopathic arthritis show complex pathological manifestations of articular lesions, involving synovitis, enthesitis, and/or abnormal proliferation of bone and cartilage.[1,2] In general, disease categories with complex pathological manifestations have been defined based on clinical criteria, but pathology of the critical lesions in disease could reflect the specific phenotypes regarding pathogenesis. Recent studies of mouse genomics to dissect pathological phenotypes could provide a new insight into this subject,[3–8] leading to the hypothesis that complex pathological phenotypes of diseases are under the control of multiple gene loci with allelic polymorphism.

According to this hypothesis, we examined remodeling of articular lesions in an MRL strain of mice bearing a Fas antigen deletion mutant, MRL/MpJ-*lpr/lpr* (MRL/lpr)[9] with genome recombination. MRL/lpr mice spontaneously develop collagen diseases involving arthritis, which resembles rheumatoid arthritis (RA) in that they exhibit many of the serological characteristics of RA, including increased serum levels of antinuclear antibodies, circulating immune complexes, and IgM- and IgG- rheumatoid factors (RF).[10–12] Moreover, the histopathological features of the articular lesions in these mice are characterized by synovial cell proliferation, inflammatory cell infiltration, granulomatous inflammation in synovial sublining tissue and pannus formation.[11,13,14] But the incidence of arthritis in these mice is <30%, and the severity is limited according to microscopic observations, moreover, the incidence of arthritis is not associated with joint swelling.

In the present study we first prepared backcross generation mice using a non-arthritis strain of mice, C3H/HeJ-*lpr/lpr* (C3H/lpr), MRL/lpr × (MRL/lpr × C3H/lpr) F1. Among these N2 mice, we observed mice developing arthritis of the ankle joints with macroscopic swelling. We then began to intercross the N2 mice by means of selection based on swelling of the ankle joints. Finally, we established a novel recombinant strain of mice, designated McH-*lpr/lpr*-RA1, which developed arthritis at a high incidence and with enthesopathy.

Correspondence: Masato Nose, MD, PhD, Department of Pathology, Division of Pathogenomics, Ehime University Graduate School of Medicine, Shitsukawa, Toon, Ehime 791-0295, Japan. Email: masanose@m.ehime-u.ac.jp

Received 3 January 2008. Accepted for publication 3 March 2008.

MATERIALS AND METHODS

Mice

MRL/lpr, C3H/lpr and MRL/Mp-+/+(MRL/+) mice were purchased from Jackson Laboratory, Bar Harbor, Maine, USA. Using the former two strains, we prepared backcross generation mice, MRL/lpr × (MRL/lpr × C3H/lpr) F1. Among the N2 mice, we observed the mice that developed arthritis, macroscopically manifested by ankle joint swelling. We then established a recombinant congenic strain of mice that developed arthritis by means of selection based on the swelling of ankle joints. From the generation F54, this recombinant congenic strain of mice was designated McH-*lpr/lpr*-RA1 (McH/lpr-RA1). These mice were housed in the Animal Research Institute of Tohoku University Graduate School of Medicine under specific pathogen-free and climate-controlled conditions with 12 h light–dark cycles, and each female and male littermate at 5 weeks of age was removed to cages (fewer than six per cage) separated from their parents to avoid fighting as much as possible.

Histopathology

At the indicated weeks of age, each mouse was bled under ether anesthesia. Sections of kidneys, heart, lungs, spleen, pancreas, salivary glands and lymph nodes were then fixed in 10% formalin in 0.01 mol/L phosphate buffer (pH 7.2) and embedded in paraffin. They were stained with HE, elastica-Masson (EM) and PAS for histological examination on light microscopy.

For ankle joints, serial sections were taken sagittally through the talus. The lesions, including calcaneus bone and anterior and posterior synovial tissue were histopathologically evaluated with the following grading system: normal, grade 0; thickening and proliferation of synovial lining, grade 1; grade 1 with granulomatous and/or fibrous lesions in synovial sublining tissue, grade 2; and grade 2 with pannus formation against bone cortex and/or bone marrow, grade 3. For knee joints, serial sections were prepared sagittally through the patella. The articular lesions including the tibia, femur, meniscus, plica alaris and capsula articularis were similarly evaluated as described in the previous section. We categorized grade 0 or 1 individuals as synovitis negative, and grade 2 or 3 individuals as synovitis positive.

The presence of ankylosis of the ankle and knee joints was also evaluated as follows: normal, grade 0; fibrous and fibrocartilage proliferative lesions in joints involving articular ligamenta and periostea, slight, grade 1; lesions similar to grade 1, moderate, grade 2; and lesions similar to grade 2, associated with bone destruction, grade 3. We categorized individuals with a score of higher than grade 1 as ankylosis positive. The incidence of vasculitis or glomerulonephritis was calculated as described previously.[15]

Flow cytometry

Lymphoid cells from the lymph nodes and spleen were examined for surface markers on flow cytometry. The cells were treated with fluorescein isothiocyanate (FITC)-conjugated rat monoclonal antibodies to Thy1.2 (clone 3D-H12; Becton Dickinson, Bedford, CA, USA), and phycoerythrin (PE)-conjugated rat monoclonal antibodies to B220 (clone RA3.6B2; PharMingen, San Diego, CA, USA), with FITC-conjugated rat monoclonal antibodies to CD4 (clone GK1.5) and PE-conjugated rat monoclonal antibodies to CD8 (clone 53–6.7; PharMingen), or with FITC-conjugated goat polyclonal antibodies to IgG or IgM (Zymed, San Francisco, CA, USA). The Fas-expressing cells were analyzed using FITC-conjugated hamster monoclonal antibodies to Fas (clone Jo2; PharMingen). These cells were analyzed on FACSCalibur using the CellQuest program (Becton Dickinson, Franklin Lakes, NJ, USA).

Immunoglobulin and autoantibody serum level

The serum levels of immunoglobulins involving IgG and IgM were quantified on single radial immunodiffusion, using goat polyclonal antimouse IgG and IgM antibodies (Zymed), respectively. The amounts of each in the serum samples were estimated from a standard curve using mouse Ig standards (Bethyl Laboratories, Montgomery, TX, USA).

The relative amounts in the serum of double-stranded DNA (dsDNA) antibodies were determined on ELISA using calf thymus DNA (type I, Sigma Chemical, St. Louis, MO, USA) and alkaline phosphatase-conjugated rabbit polyclonal antibodies to mouse IgG (AP-antimouse IgG; Sigma) according to a method previously described.[16] Rheumatoid factor was measured as IgG antibodies that specifically bound to the recombinant Fc fragments derived from human IgG1.[17]

Statistical analysis

The association of each strain with the incidence of synovitis or ankylosis was evaluated using Fisher's exact test. The difference between each strain in the weight of spleen, axillary lymph nodes, and serum levels of IgG, IgM and autoantibodies was evaluated on Student's *t*-test. $P < 0.01$ was considered to be significant.

RESULTS

Higher incidence of arthritis and enthesopathy

Ankle joint swelling of McH/lpr-RA1 mice was significantly observed at later than 16 weeks of age (Fig. 1). At 20 weeks

of age, these mice microscopically showed severe inflammatory synovitis with pannus formation resembling that in MRL/lpr mice (Fig. 2a), but the incidence of synovitis in the ankle joints was remarkably higher (60.3%) than in the MRL/lpr mice (8.0%; Table 1). Similar lesions were frequently observed in the knee joints (Fig. 2b). The incidence of synovitis of knee joints in McH/lpr-RA1 mice was not significantly higher than that in the MRL/lpr mice (Table 1).

Among McH/lpr-RA1 mice, many individuals developed ankylosis in their ankle and knee joints. Ankylosis in this strain of mice was characterized by fibrous and fibrocartilage proliferative lesions in the joints involving articular ligamenta and periostea, partly occupying the joint space, resembling enthesopathy (Fig. 2c–f). These lesions seemed to be specific for McH/lpr-RA1 mice because no MRL/lpr and C3H/lpr mice developed these lesions (Table 2). Sex difference in ankylosis of McH/lpr-RA1 mice was not a significant factor in the ankle or knee joints ($P = 0.073$ and $P = 0.093$, respectively), thus indicating that ankylosis in these mice might not result from an aggressive behavior as is generally considered in male mice. It seemed that synovitis, at least in ankle joints, developed prior to ankylosis at 8 week of age because ankylosis in ankle joints was never observed in any McH/lpr-RA1 mice at 8 weeks of age (Tables 1,2). But the correlation between the synovitis grades and ankylosis grades, at least in the ankle joints at 20 weeks of age, was not significant (female, correlation coefficient: $r = -0.167$; male; $r = 0.404$; total, $r = 0.183$).

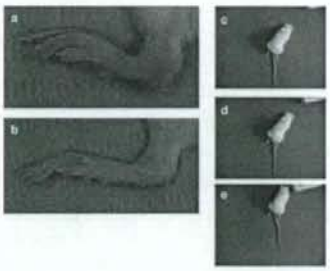

Figure 1 Joint swelling in McH/lpr-RA1 mice. A male McH/lpr-RA1 mouse at 16 week of age shows (**a**) significant swelling of ankle joint, compared with (**b**) an age-matched male MRL/lpr mouse. (**c–e**) Pictures clipped from the video film showing crippled walking of a male McH/lpr-RA1 mouse at 20 weeks of age due to ankylosis.

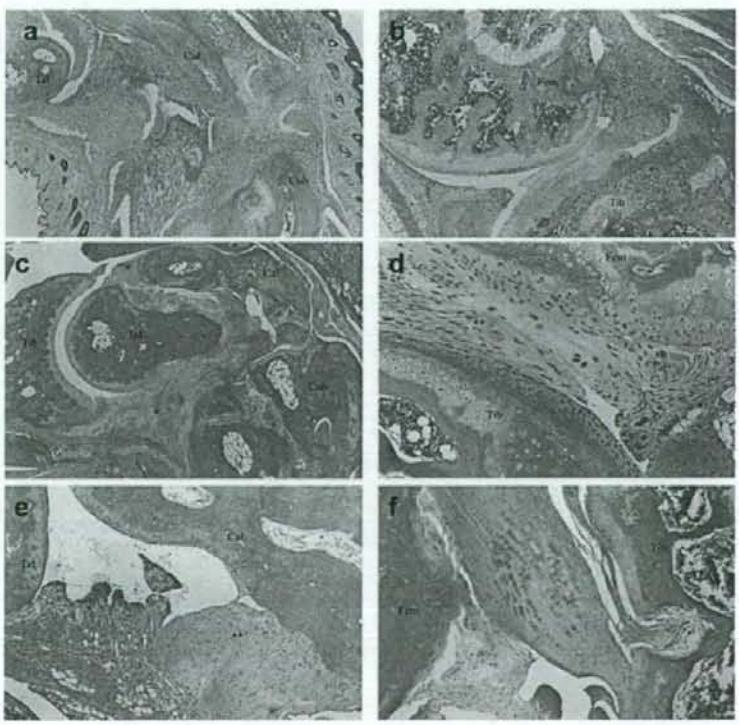

Figure 2 Representative histopathological features of articular lesions in McH/lpr–RA1 mice. (**a,c,e**) Ankle joints and (**b,d,f**) knee joints (HE). Cal, calcaneus; Cub, cuboidal bone; Fem, femur; Tal, talus; Tib, tibia. (**a**) Male mouse at 20 weeks of age shows severe inflammatory proliferative lesions of synovial tissues with pannus formation, evident against talus, calcaneus and cubic bones (synovitis grade 3). (**b**) Male mouse at 20 weeks of age developed synovitis corresponding to synovitis grade 3 showing severe pannus formation (*), invading into tibia bone. (**c**) Ankylosis in a male mouse at 20 weeks of age, characteristic of the proliferative lesions of fibrocartilage, but not hyaline cartilage, especially marked in articular ligament around talus bone (*; ankylosis grade 3). (**d**) Ankylosis of a male mouse at 8 weeks of age showing fibrocartilaginous change of the intra-articular ligament (**; ankylosis grade 1) associated with grade 1 synovitis (*). (**e**) Synovitis with inflammatory fibrosis in the sublining region (*; grade 2) and ankylosis with destruction of calaneus (**; grade 3) in a male mouse at 20 weeks of age. (**f**) Fibrocartilaginous change of intra-articular ligament, associated with the growth of chondrocytes (ankylosis), and synovitis with pannus (*), characteristically with the presence of osteoclasts, in a male mouse at 20 weeks of age.

Table 1 Incidence of synovitis in McH/lpr-RA1, MRL/lpr and C3H/lpr mice

	Grade of synovitis					
	0	1	2	3	Incidence of positive mice, *n* (%)†	
Ankle joints						
McH/lpr-RA1 (20 week old)						
Female	0	8	0	12	12/20	(60.0)
Male	0	17	1	25	26/43	(60.5)
Total	0	25	1	37	38/63	(60.3)‡
McH/lpr-RA1 (8 week old)						
Female	0	17	0	0	0/17	(0.0)
Male	0	15	1	1	2/17	(11.8)
Total	0	32	1	1	2/34	(5.9)
MRL/lpr (20 week old)						
Female	8	2	0	1	1/11	(9.1)
Male	9	4	1	0	1/14	(7.1)
Total	17	6	1	1	2/25	(8.0)
C3H/lpr (20 week old)						
Female	17	8	0	0	0/25	(0.0)
Male	20	1	0	2	2/23	(0.1)
Total	37	9	0	2	2/48	(4.2)
Knee joints						
McH/lpr-RA1 (20 week old)						
Female	0	2	0	18	18/20	(90.0)§
Male	1	19	1	22	23/43	(53.5)
Total	1	21	1	40	41/63	(65.1)#
McH/lpr-RA1 (8 week old)						
Female	0	5	0	12	12/17	(70.6)
Male	0	7	0	10	10/17	(58.8)
Total	0	12	0	22	22/34	(64.7)
MRL/lpr (20 week old)						
Female	6	0	0	5	5/11	(45.5)
Male	5	3	0	6	6/14	(42.9)
Total	11	3	0	11	11/25	(44.0)
C3H/lpr (20 week old)						
Female	25	0	0	0	0/25	(0.0)
Male	22	1	0	0	0/23	(0.0)
Total	47	1	0	0	0/48	(0.0)

‡$P = 0.0014$ vs MRL/lpr mice, Fisher's exact test; §$P = 0.215$ vs female MRL/lpr mice, Fisher's exact test; #$P = 0.228$ vs MRL/lpr mice, Fisher's exact test.

†No. synovitis-positive mice (grades 2 and 3)/total number examined (%).

Development of vasculitis, but no glomerulonephritis

McH/lpr-RA1 mice coincidentally developed vasculitis, but not glomerulonephritis. The incidence of vasculitis in kidney was similar to that in MRL/lpr mice at 20 weeks of age (McH/lpr-RA1, 63/63; MRL/lpr, 17/25; $P = 0.186$). The histopathological features of vasculitis were characteristic of granulomatous arteritis, similar to those of MRL/lpr mice (data not shown). In contrast, the incidence of glomerulonephritis was significantly different (McH/lpr-RA1, 12/63; MRL/lpr, 17/25; $P < 0.004$). This may be the reason why the McH/lpr-RA1 mice lived remarkably longer than the MRL/lpr mice.

Dissociation from lymphoproliferative disorder

Importantly, all mice of the McH/lpr-RA1 strain had only mild splenomegaly and lymphadenopathy (spleen, 0.275 ± 0.145 g; lymph nodes, 0.174 ± 0.164 g), different from the original strains of MRL/lpr (spleen, 0.531 ± 0.199 g, $P < 0.001$; lymph nodes, 0.730 ± 0.298 g, $P < 0.001$) and C3H/lpr mice (spleen, 0.562 ± 0.189 g, $P < 0.001$; lymph nodes, 0.875 ± 0.288 g, $P < 0.001$), although there was no difference between MRL/lpr and C3H/lpr mice in spleen and lymph nodes ($P > 0.01$).

The accumulation of $Thy1^+B220^+$ T cells into the spleen and lymph nodes, which is a characteristic phenotype of the *lpr* gene,[18] was not remarkable, in comparison to that in MRL/lpr and C3H/lpr mice (Fig. 3a). This seemed to reflect the decrease of the double negative ($CD4^-CD8^-$) T cells in the spleen and lymph nodes and, in contrast, the increase of $CD4^+$ T cells and especially $CD8^+$ T cells (Fig. 3b). As a result, the CD4/CD8 ratio of spleen cells and lymph node cells was found to be remarkably lower in the McH/lpr-RA1 mice than in the MRL/lpr or C3H/lpr mice, although the high CD4/CD8 ratio in *lpr*-bearing mice is thought to result from the absence of Fas-mediated apoptosis in $CD4^+$ T cells.[15] But the expres-

Table 2 Incidence of ankylosis in McH/lpr-RA1, MRL/lpr and C3H/lpr mice

	Grade of ankylosis					
	0	1	2	3	Incidence of positive mice, *n* (%)†	
Ankle joints						
McH/lpr-RA1 (20 weeks old)						
Female	11	6	3	0	9/20	(45.0)
Male	2	9	14	18	41/43	(95.3)
Total	13	15	17	18	50/63	(79.4)**
McH/lpr-RA1 (8 weeks old)						
Female	17	0	0	0	0/17	(0.0)
Male	17	0	0	0	0/17	(0.0)
Total	34	0	0	0	0/34	(0.0)
MRL/lpr (20 weeks old)						
Female	11	0	0	0	0/11	(0.0)
Male	14	0	0	0	0/14	(0.0)
Total	25	0	0	0	0/25	(0.0)
C3H/lpr (20 weeks old)						
Female	25	0	0	0	0/25	(0.0)
Male	23	0	0	0	0/23	(0.0)
Total	48	0	0	0	0/48	(0.0)
Knee joints						
McH/lpr-RA1 (20 weeks old)						
Female	8	10	2	0	12/20	(60.0)
Male	31	11	1	0	12/43	(27.9)
Total	39	21	3	0	24/63	(38.1)***
McH/lpr-RA1 (8 weeks old)						
Female	16	1	0	0	1/17	(5.9)
Male	16	1	0	0	1/17	(5.9)
Total	32	2	0	0	2/34	(5.9)
MRL/lpr (20 weeks old)						
Female	11	0	0	0	0/11	(0.0)
Male	14	0	0	0	0/14	(0.0)
Total	25	0	0	0	0/25	(0.0)
C3H/lpr (20 weeks old)						
Female	25	0	0	0	0/25	(0.0)
Male	23	0	0	0	0/23	(0.0)
Total	48	0	0	0	0/48	(0.0)

**$P = 0.001$ vs MRL/lpr mice, Fisher's exact test; ***$P < 0.0001$ vs MRL/lpr mice, Fisher's exact test.
†No. positive mice (grades 1, 2 and 3)/total number examined (%).

sion of Fas in splenic cells and lymph node cells was remarkably lower than that in MRL/+mice: almost at the same level as that in MRL/lpr and C3H/lpr mice (Fig. 3c).

Dissociation from autoimmune traits

The serum levels of IgG in McH/lpr-RA1 mice were significantly lower than those of MRL/lpr and C3H/lpr mice, whereas the IgM level was similar to that in MRL/lpr mice (Fig. 4) although the number of IgG or IgM positive cells in the spleen and lymph node in this strain were relatively higher than those of MRL/lpr and C3H/lpr mice (Fig. 3d,e).

The serum levels of both IgG anti-dsDNA antibodies and IgG rheumatoid factors in McH/lpr-RA1 mice were remarkably low in comparison to those of both MRL/lpr and C3H/lpr mice (Fig. 5). These titers were almost the same in the McH/lpr-RA1 mice at 8 weeks of age (data not shown).

DISCUSSION

In the present study we established a novel recombinant congenic strain of mice, McH/lpr-RA1, which was started from the MRL/lpr × (MRL/lpr × C3H/lpr) F1 generation, by means of selection based on swelling in the ankle joints. In this strain, synovitis developed in the ankle joints at a higher incidence than that in the MRL/lpr mice, and ankylosis manifested by enthesopathy developed in the ankle and knee joints. This supports the idea that arthritis is controlled by polygenic inheritance. Namely, a particular genome combination with C3H/lpr alleles accelerates the incidence of synovitis and produces enthesopathy.

Such a genome recombination was also useful for evaluating several serological parameters that might be responsible for the development of diseases. McH/lpr-RA1 mice had a lower level of both IgM and IgG despite the presence of the *lpr* gene (Fig. 4a,b), and their IgG autoantibodies were fewer than in MRL/lpr and C3H/lpr mice (Fig. 5a,c). In previous

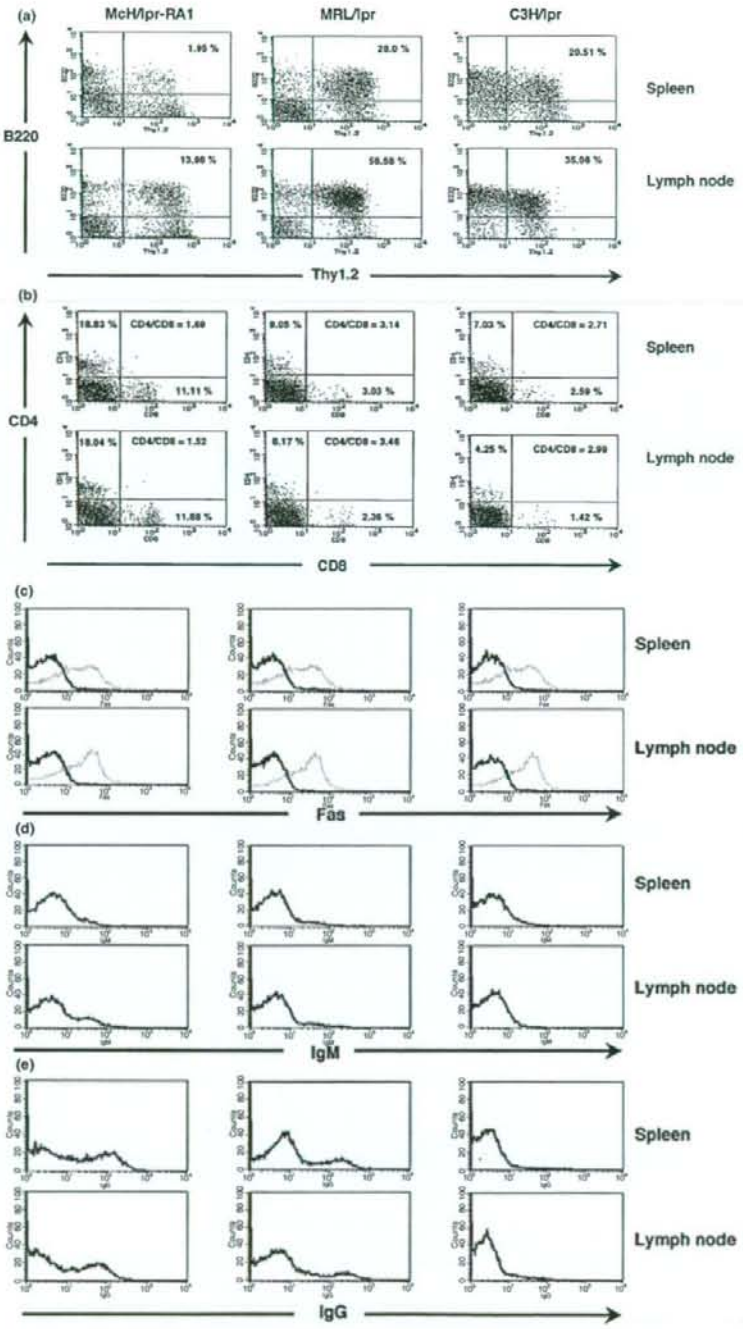

Figure 3 Flow cytometry of lymphocytes from spleen and lymph nodes from 20-week-old McH/lpr-RA1, MRL/lpr and C3H/lpr mice. Representative profiles of the cells were analyzed based on the expression of (**a**) Thy1.2 and B220, (**b**) CD4 and CD8, (**c**) Fas, (**d**) IgM and (**e**) IgG. For Fas antigen expression, 20-week-old MRL/+mice were used as controls (fine lines in c).

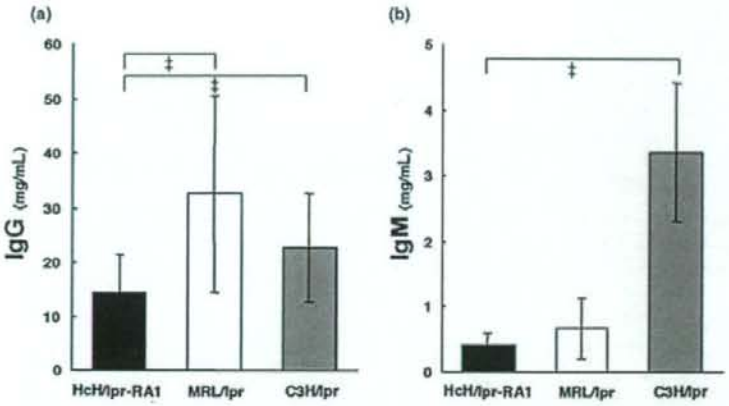

Figure 4 The serum levels of (a) IgG and (b) IgM. McH/lpr-RA1 ($n = 22$), MRL/lpr ($n = 20$) and C3H/lpr ($n = 20$) mice at 20 weeks of age (mean and SEM). ‡$P < 0.005$.

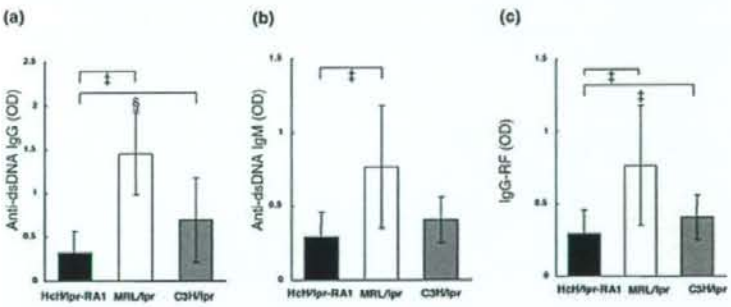

Figure 5 Serum levels of (a) IgG and (b) IgM anti-dsDNA antibodies and (c) IgG rheumatoid factors (RF). McH/lpr-RA1 ($n = 22$), MRL/lpr ($n = 20$) and C3H/lpr ($n = 20$) mice at 20 weeks of age (mean and SEM). OD, optical density. ‡$P < 0.005$; §$P < 0.01$.

studies in MRL/lpr mice, high serum levels of IgG rheumatoid factor seemed to play a critical role in the development of arthritis.[11,19] But it became clear in the present study that high serum levels of IgG rheumatoid factor as found in MRL/lpr mice are not necessary for the development of arthritis in McH/lpr-RA1 mice. As a result, the pathogenetic role of IgG rheumatoid factor on arthritis in MRL/lpr mice therefore needs to be re-evaluated.

Moreover, lymphoproliferative disorders manifested by splenomegaly and lymphadenopathy decreased in McH/lpr-RA1 mice in comparison to those in MRL/lpr and C3H/lpr mice, although the Fas deletion levels on the cell surface were almost the same among these three *lpr* strains (Fig. 3c). Throughout the repeated intercrossing for the establishment of the recombinant congenic strain, we observed that the lymph node weights seemed to decrease for each generation. Correspondingly, the accumulation of $Thy1^+B220^+$ T cells into spleen and lymph nodes decreased (Fig. 3a) while the ratio of CD4/CD8 decreased (Fig. 3b). This indicates that T-cell subsets in the periphery might be controlled by an allelic combination in the *lpr* mice, and that a mechanism besides Fas-mediated apoptosis has become accelerated in this strain. The expression levels of tumor necrosis factor-α should be further studied as one of the candidates inducing apoptosis,[20] which might also correlate with the higher incidence of synovitis in this strain.

It is important to elucidate whether ankylosis in the McH/lpr-RA1 mice might be the result of synovitis. In general, synovitis associated with pannus formation is though to lead ankylosis in RA, mainly characterized by the replacement of the joint surface by fibrous tissue derived from the invading pannus. Ankylosis in this strain of mice, however, seems to be due to enthesopathy, which was histopathologically manifested by the fibrous and fibrocartilaginous proliferation of enthesis, the site of insertion of a tendon, ligamenta or articular capsule into bone, similar to that previously described.[21] If that is the case, then synovitis in this strain of mice might be a result of secondary synovitis following enthesopathy.[22] But this is unlikely considering that the correlation between the synovitis grades and the ankylosis grades in the ankle joints of McH/lpr-RA mice at 20 weeks of age was not significant, and also that MRL/lpr mice developed synovitis in knee joints as often as McH/lpr-RA1 mice, but never developed ankylosis (Tables 1,2). As a result, the development of enthesopathy may be genetically independent from synovitis. Similar lesions to enthesopathy in McH/lpr-RA1 mice can be observed in male

DBA/1 mice that spontaneously develop the lesions in their ankles or lower extremities at older than 4 months of age, but these mice are not associated with severe synovitis.[23,24] We recently found that the severity and early onset of enthesopathy in DBA/1 mice were accelerated by a gene locus in an MRL allele, which was localized on chromosome 10 and designated Adm1.[25] This locus in McH/lpr-RA1 mice was an MRL homozygote, which involves several candidate genes mediating cellular proliferation and differentiation such as β2 integrin, basigin and macrophage migration inhibitory factor (MIF). In humans, *MIF* and *ITGB2* (β2 integrin) are associated with juvenile idiopathic arthritis.[26,27]

The present findings thus suggest that a diversity of pathological manifestations of arthritic lesions might be involved in a common genomic spectrum of collagen disease including RA, spondylarthropathy and juvenile idiopathic arthritis, especially enthesitis-related arthritis.[2]

ACKNOWLEDGMENTS

The authors are indebted to Ms S. Terasaki for technical help in animal care, and Ms E. Kondo and M. Terada for assistance with histopathology. This study was supported by Grant-in Aid for the Scientific Research Funds of the Ministry of Education, Science and Culture of Japan (S.M. 15390607, M.N. 18390123).

REFERENCES

1 Maini RN, Zvaifler NJ. Rheumatoid arthritis and spondyloarthropathy. In: Klippel JH, Dieppe PA, eds. *Rheumatology*. London: Mosby, 1994; 3.1.1–3.40.2.
2 Petty RE, Southwood TR, Baum J *et al.* Revision of the proposed classification criteria for juvenile idiopathic arthritis: Durban, 1997. *J Rheumatol* 1998; **25**: 1991–4.
3 Nose M, Nishimura M, Kyogoku M. Analysis of granulomatous arteritis in MRL/Mp autoimmune disease mice bearing lymphoproliferative genes. The use of mouse genetics to dissociate the development of arteritis and glomerulonephritis. *Am J Pathol* 1989; **135**: 271–80.
4 Nose M, Nishimura M, Ito MR, Itoh J, Shibata T, Sugisaki T. Arteritis in a novel congenic strain of mice derived from MRL/lpr lupus mice. *Am J Pathol* 1996; **149**: 1763–9.
5 Nishimura H, Nose M, Hiai H, Minato N, Honjo T. Development of lupus-like autoimmune diseases by disruption of the PD-1 gene encoding an ITIM motif-carrying immunoreceptor. *Immunity* 1999; **11**: 141–51.
6 Nose M, Nishihara M, Fujii H. Genetic basis of the complex pathological manifestations of collagen disease: Lessons from MRL/lpr and related mouse models. *Int Rev Immunol* 2000; **19**: 473–98.
7 Nishimura H, Okazaki T, Tanaka Y *et al.* Autoimmune dilated cardiomyopathy in PD-1 receptor-deficient mice. *Science* 2001; **291**: 319–22.
8 Kamogawa J, Terada M, Mizuki S *et al.* Arthritis in MRL/lpr mice is under the control of multiple gene loci with an allelic combination derived from the original inbred strains. *Arthritis Rheum* 2002; **46**: 1067–74.
9 Murphy ED, Roths JB. Autoimmunity and lymphoproliferation: Induction by mutant gene *lpr*, and acceleration by a male-associated factor in strain BXSB mice. In: Rose NR, Bigazzi PE, Warner NL, eds. *Genetic Control of Autoimmune Disease*. New York: Elsevier North Holland, 1978; 207–20.
10 Izui S, Eisenberg RA. Circulating anti-DNA-rheumatoid factor complexes in MRL/1 mice. *Clin Immunol Immunopathol* 1980; **15**: 536–51.
11 Hang L, Theofilopoulos AN, Dixon FJ. A spontaneous rheumatoid arthritis-like disease in MRL/1 mice. *J Exp Med* 1982; **155**: 1690–701.
12 Nardella FA, Teller DC, Izui S, Mannik M. Self-associating IgG rheumatoid factors in MRL/1 autoimmune mice. *Arthritis Rheum* 1982; **27**: 1165–73.
13 O'Sullivan FX, Fassbender HG, Gay S, Koopman WJ. Etiopathogenesis of the rheumatoid arthritis-like disease in MRL/1 mice. I. The histomorphologic basis of joint destruction. *Arthritis Rheum* 1985; **28**: 529–56.
14 Tarkowski A, Jonsson R, Holmdahl R, Klareskog L. Immunohistochemical characterization of synovial cells in arthritic MRL-*lpr*/*lpr* mice. *Arthritis Rheum* 1987; **30**: 75–82.
15 Wang Y, Nose M, Kamoto T, Nishimura M, Hiai H. Host modifier genes affect mouse autoimmunity induced by the *lpr* gene. *Am J Pathol* 1997; **151**: 1791–8.
16 Takahashi S, Nose M, Sasaki J, Yamamoto T, Kyogoku M. IgG3 production in MRL/lpr mice is responsible for development of lupus nephritis. *J Immunol* 1991; **147**: 515–20.
17 Nose M, Takano R, Nakamura S, Arata Y, Kyogoku M. Recombinant Fc of human IgG1 prepared in an *Escherichia coli* system escapes recognition by macrophages. *Int Immunol* 1990; **2**: 1109–12.
18 Morse HC III, Davidson WF, Yetter RA, Murphy ED, Roths JB, Coffman RL. Abnormalities induced by the mutant gene lpr: Expansion of unique lymphocyte subset. *J Immunol* 1982; **129**: 2612–15.
19 Otto JM, Cs-Szabo G, Gallagher J *et al.* Identification of multiple loci linked to inflammation and autoantibody production by a genome scan of a murine model of rheumatoid arthritis. *Arthritis Rheum* 1999; **42**: 2524–31.
20 Zheng L, Fisher G, Miller RE, Peschon J, Lynch DH, Lenardo MJ. Induction of apoptosis in mature T cells by tumour necrosis factor. *Nature* 1995; **377**: 348–51.
21 Niepel GA, Sitaj S. Enthesopathy. *Clin Rheum Dis* 1979; **5**: 857–87.
22 McGonagle D, Gibbon W, Emery P. Classification of inflammatory arthritis by enthesitis. *Lancet* 1998; **352**: 1137–40.
23 Holmdahl R, Jansson L, Andersson M, Jonsson R. Genetic, hormonal and behavioural influence on spontaneously developing arthritis in normal mice. *Clin Exp Immunol* 1992; **88**: 467–72.
24 Nordling C, Karlsson Parra A, Jansson L, Holmdahl R, Klareskog L. Characterization of a spontaneously occurring arthritis in male DBA/1 mice. *Arthritis Rheum* 1992; **35**: 717–22.
25 Oishi H, Miyazaki T, Mizuki S *et al.* Accelerating effect of an MRL gene locus on the severity and onset of arthropathy in DBA/1 mice. *Arthritis Rheum* 2005; **52**: 959–66.
26 Donn R, Alourfi Z, De Benedetti F *et al.* Mutation screening of the macrophage migration inhibitory factor gene: Positive association of a functional polymorphism of macrophage migration inhibitory factor with juvenile idiopathic arthritis. *Arthritis Rheum* 2002; **46**: 2402–9.
27 Fujita K, Kobayashi K, Okino F. Juvenile rheumatoid arthritis in two siblings with congenital leukocyte adhesion deficiency. *Eur J Pediatr* 1988; **148**: 118–19.

ACOUSTIC CHARACTERISTICS OF ULTRASOUND IN WATER CONTAINING LIPID MICROBUBBLES

R. Imai, H. Nakagawa, T. Kanagawa, M. Watanabe and S. Fujikawa*
Division of Mechanical and Space Engineering,
Graduate School of Engineering, Hokkaido University, Sapporo, 060-8628, Japan

ABSTRACT. The resonant frequencies of lipid bubbles are measured from attenuation of ultrasound pulse propagating through the test cell filled with normal saline or lipid bubble solution. The attenuation spectrum has two dominant peaks in the frequency range of 0 through 15 MHz due to the energy absorption by lipid bubble resonant oscillations. The two peaks of attenuation spectrum are observed near the bands of 1.4 MHz and 11.5 MHz, respectively. The peaks of attenuation spectrum decrease with the decrease in the concentration of the lipid bubble solution. Furthermore, the strong attenuation is confirmed to be hardly affected by the length through the lipid bubbles. We conclude that the two peaks in the attenuation spectrum obtained are related to the effect of the existence of lipid bubbles.

Keywords: *Ultrasound, Lipid microbubble, Drug delivery system*

INTRODUCTION

Bubbles have been widely used in various fields, for instance, from marine engineering to medical engineering. One of the most characteristic features observed in the practical bubble application is a wide range of bubble diameter. Diameters of bubbles are of the order of millimeters when bubbles are used for the drag reduction of large vessel. On the other hand, they are of the order of nanometers when bubbles are used for clinical applications such as the contrast agents.

In the field of medical engineering, the application of bubbles to Drug Delivery System (DDS) has attracted great attention as the administration of next generation. DDS with bubbles of nanometer size is expected to be a noninvasive clinical treatment. Capsules of nanometer size, which contain exogenous gene such as anticancer drug, are administered in blood. These capsules are transported to target sites and impregnate in the disorder cells efficiently.

There exist bubbles wrapped in biomedical materials, i.e., lipid. The lipid bubbles are used as the transport carrier of DDS. However, dynamic properties of these lipid bubbles are not yet made clear. DDS with lipid bubbles uses actively the resonance of bubbles in order to increase the efficiency of gene injection in the disordered cell, because oscillations of lipid bubbles are easily excited with sufficiently small driving forces at resonant conditions.

In this study, acoustic characteristics of lipid bubbles are experimentally investigated in the vicinity of the resonance. The resonant frequencies of lipid bubbles are evaluated by measuring the attenuation of the propagating broadband ultrasound waves through the water containing lipid bubbles.

EXPERIMENTAL METHOD

Lipid bubble

* Corresponding author: Prof. S. Fujikawa
Phone: + (81)-11-706-6429, Fax: + (81)-11-706-6429
E-mail address: fujikawa@eng.hokudai.ac.jp

We use lipid bubbles in a liquid. A lipid bubble is composed of a kind of shell made of lipid layer, in which both gas and liquid are contained. The lipid bubble is made from a liposome. Figure 1 shows schematic diagrams of a lipid bubble. The liposome used in the present experiment is first made of lipid with DSPC (DiStearoyl Phosphatidyl Choline) and then modified by PEG (PolyEthlen Glycol Distearate). With the treatment, the liposome can exist stably in blood. The liposome becomes easily incorporated with ligand that is able to bind disease-related markers on bubble surfaces.

The liposome is produced by the reverse phase evaporation method. The inside of liposome produced by this method is liquid phase (Figure 1 (a)); hence liquid should be replaced by C_3F_8 (Perfluorocarbon) gas (Figure 1 (b)). The C_3F_8 gas is first injected into a glass receptacle containing a liposome solution, and then the receptacle is wobbled using an ultrasonic cleaner (Ultrasound cleaner 2510-J-DTH, Bransonic Co., Ltd.) until the solution in the receptacle becomes opaque. As shown in Figure 1 (b), it is supposed that replacement from the contained liquid to the gas within the liposome is attained by micelle formation inside the liposome [1]. The C_3F_8 gas enables lipid bubbles containing this gas to be used as an ultrasound contrast agent [2]. It is also necessary to equalize the size distribution of lipid bubbles by using the 20 kHz ultrasound probe. The lipid bubbles with larger diameters are assumed to be destroyed by this procedure. Figure 2 shows the distribution of lipid bubble diameter.

The solution containing lipid bubbles is diluted with the PBS (Phosphate Buffered Saline), and thus, solutions of different concentrations are obtained. The stock solution of lipid bubbles before diluted contains DSPC of 1 mg in its 1 ml. In this study, lipid bubble solutions with the concentration of 1000 ppm, 1333 ppm, 2000 ppm, and 4000 ppm are used. The experimental test cell which is the container made of the Polyvinylidene Chloride film (Saran Wrap, Asahi Kasei Co., Ltd.) is filled with lipid bubble solution. Ultrasound passes through this film.

Figure 3 shows the scanning electron micrograph of the liposome.

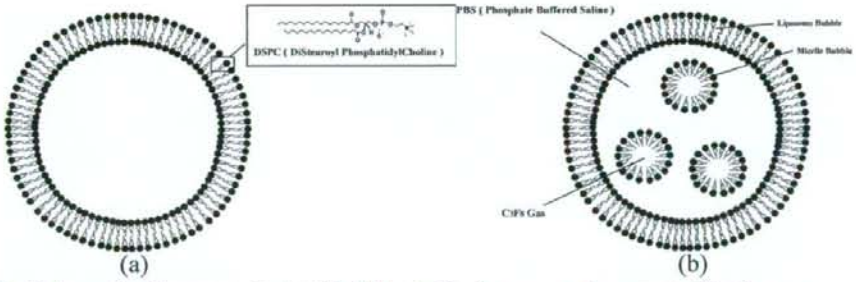

Figure 1. Schematic diagrams of a lipid bubble: (a) before gas replacement, (b) after gas replacement of liquid phase inside a liposome.

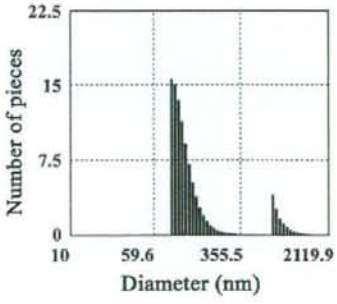

Figure 2. Distribution of lipid bubble diameter.

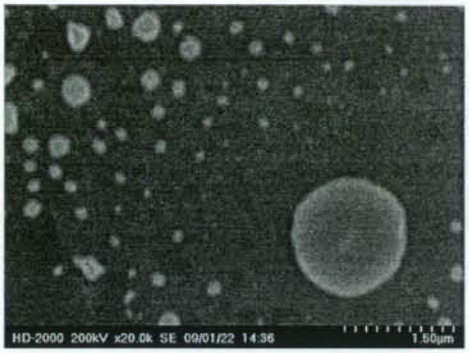

Figure 3. The scanning electron micrograph of the liposome.

Experimental apparatus and method

Experimental apparatus

Figure 4 shows the experimental apparatus, which is similar to that used by Hoff et al. [3]. This apparatus consists of a pulser/receiver, a coaxial cable relay for selecting transducers, four transducers (Panametrics Videoscan V306-SU, V382-SU, V326-SU and V312-SU), and a digital oscilloscope (LeCroy9410, LeCroy Co., Ltd.). The pulser/receiver and oscilloscope were connected to a PC.

Central frequencies of four types of broadband ultrasound transducers are 2.25MHz, 3.5MHz, 5.0MHz, and 10.0MHz, respectively. The four transducers are unfocused, 2.25 MHz with 13 mm aperture diameter, 3.5 MHz with 13 mm aperture, 5.0 MHz with 10 mm aperture, and 10.0 MHz with 6 mm aperture diameter. They are mounted in parallel in a water tank made of acrylic.

The test cell is filled with normal saline or the diluted lipid bubble solution. The lengths of the cell are 31.5 mm or 15.0 mm, and the distances from transducers to the experimental cell are 100 mm. The back wall of the water tank acts as an acoustic reflector, and is placed 150 mm from the transducer faces as shown in Figure 4. This acoustic reflector is made of steel.

Experimental method

The transducers are excited by the pulser which sends broadband ultrasound short pulses at 50 pulses per second. These pulses propagate through the experimental cell containing a lipid bubble solution separated from the ambient water by a very thin plastic film. These pulses are reflected at the back wall of the water tank, and then received by the transducer again. That is, the pulses pass through the cell twice; hence the total sound path lengths through the cells of 31.5 mm and 15.0 mm become 63.0 mm and 30.0 mm, respectively. The received pulses are amplified by the receiver and transferred to the oscilloscope. The oscilloscope is set to display only the reflection off the back wall of the chamber. The pulses are digitized in the oscilloscope at a sampling rate of 20 GS/s, and transferred to PC.

Signal processing of the received pulses is carried out using MATLAB software (The Math Works, Inc., Natick, MA). The power spectra are calculated by the Fast Fourier Transformation of received pulses in the cases of with and without lipid bubbles in the cell, respectively. Figure 5 shows an example of received pulses and their power spectra, without and with lipid bubbles in the cell with 31.5 mm in length. The attenuation spectra are calculated by the normalization, i.e., dividing the difference of power spectra both with and without lipid bubbles by the total sound path length through the cell, which is either 63.0 mm or 30.0 mm.

The evaluation ranges of broadband ultrasound transducers are from 1.4 to 3.0MHz, from 2.0 to 5.0MHz, from 3.0 to 8.0MHz, and from 6.0 to 14.0MHz, respectively, which correspond to their central frequencies 2.25MHz, 3.5MHz, 5.0MHz, and 10MHz. The overlaps of the curves obtained by different transducers assure the consistency of the experiment.

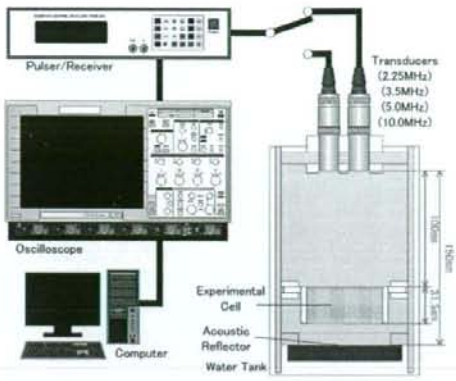

Figure 4. Schematic of the experimental apparatus.

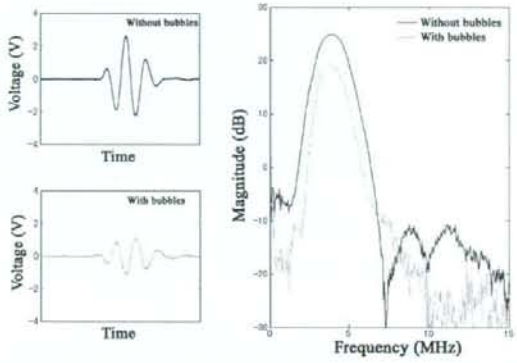

Figure 5. An example of received pulses and their power spectra measured with 3.5 MHz transducer. The left diagrams show received pulses passed through the cell twice: The upper and lower figures shows received pulses without and with lipid bubbles, respectively. The right diagram shows their power spectra, without and with lipid bubbles in the experimental cell.

RESULTS

First, we measured power spectra both with and without lipid bubbles, and calculated the attenuation spectrum, which is defined as the division of the difference between them by the total sound path length through the experimental cell, with both acoustic energy and the path length of the experimental call fixed as 100 μJ and 31.5 mm, respectively. The attenuation spectrum, which is used as the index of the difference of the acoustic characteristics between with and without lipid bubbles, is shown in Figure 6 in the case of the lipid bubble solution concentration of 1333 ppm.

Figure 6 is a typical example of the attenuation spectrum. It should be emphasized that, in this frequency range (0-15 MHz), this attenuation spectrum has two peaks. The larger attenuation is observed around the frequency of 1.4 MHz, the other is observed around the frequency of 11.5 MHz. It is understood that the existence of these peaks in the attenuation spectrum is due to the acoustic energy absorption by the lipid bubbles with resonant oscillations; hence the resonant frequencies of the solution of lipid bubbles are evaluated as approximately around the frequencies of 1.4 MHz and 11.5 MHz. These two peaks should be closely related with the distribution characteristics of the lipid bubble diameter, as already shown in Figure 2. Thereafter, these two peaks of the attenuation spectrum are discussed in the context of the acoustic characteristics of the lipid bubbles.

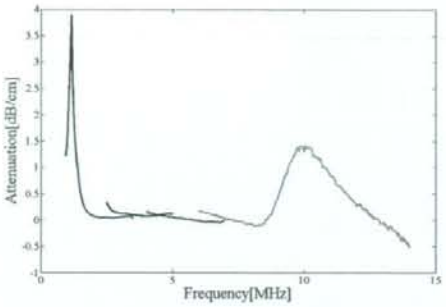

Figure 6. Acoustic attenuation spectra: with acoustic energy of 100 μJ, cell thickness of 31.5 mm, concentration of 1333 ppm.

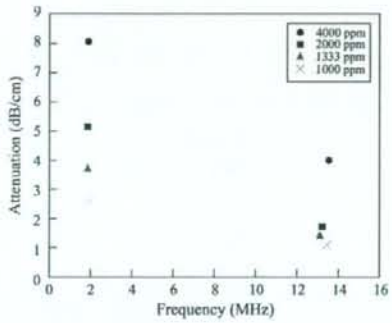

Figure 7. Peak attenuation with acoustic energy of 100 μJ, cell thickness is 31.5 mm, concentrations of 1000 ppm, 1333 ppm, 2000 ppm, and 4000 ppm.

Figure 7 shows the effects of concentration of the lipid bubble solution on the magnitudes of the attenuation at the two peaks of the attenuation spectrum. Here, the acoustic energy and the length of the experimental cell are fixed as 100 μJ and 31.5 mm, as before. Four types of lipid bubble solutions with the concentration of 1000 ppm, 1333 ppm, 2000 ppm, and 4000 ppm are used. It should be noted that the magnitudes of the attenuation at both of the two peaks decrease with the decrease in the concentration of the lipid bubble solution. The concentration of the solution is proportional to number of lipid bubbles per unit volume, and consequently to the amount of energy absorbed by the resonant frequencies of the lipid bubbles.

In order to discuss the effects of the total sound path length, we compare the attenuation spectra obtained by using two cells with different lengths of 31.5 mm and 15.0 mm, respectively. Figure 8 shows the effects of cell length on the magnitude of the attenuation at the two peaks of the attenuation spectrum, in the case that the acoustic energy is 100 μJ and the concentration of the lipid bubble solution is 2000 ppm. There exist little influences of the difference in the cell length; hence the magnitude of the attenuation peak is independent of the total path length through the lipid bubble solution.

As has been already discussed, the two dominant peaks in the attenuation spectrum obtained by this experiment are related to the resonance of the lipid bubbles. A resonant frequency increases with the decrease in the diameter of bubbles. Therefore, the resonant frequency observed in the vicinity of 1.4 MHz and 11.5 MHz may be contributed by lipid bubbles with diameter of 1.5 μm of 200 nm, respectively. It should be noted that this discussion should be improved by incorporating the multiple bubble effects.

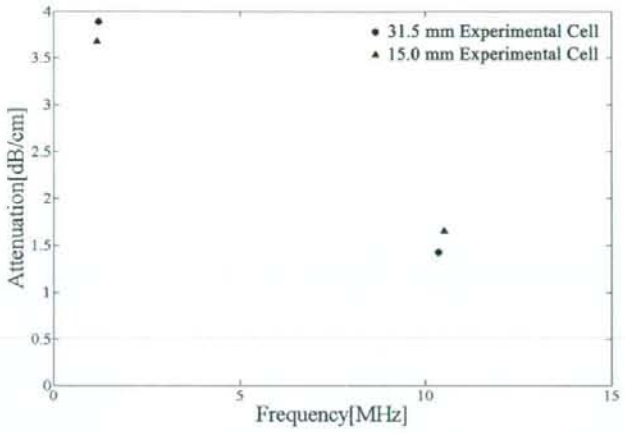

Figure 8. Acoustic attenuation spectra with acoustic energy of 100 μJ concentration of 1333 ppm, cell thickness of 31.5 mm and 15.0 mm.

CONCLUSIONS

We have experimentally studied the resonant frequencies of the lipid bubbles and obtained the following results:

(1) The attenuation spectrum, which is defined as the division of the difference of power spectra between with and without lipid bubbles by the total sound path length through the experimental cell, has two dominant peaks.

(2) The strong attenuations are observed at two different frequencies, around 1.4 MHz and 11.5 MHz, respectively.

(3) The strong attenuation decreases with the decrease in the concentration of the lipid bubble solution.

(4) The strong attenuation is independent of the path length through the lipid bubbles.

ACKNOWLEDGEMENTS

This work was carried out by the aid of Research on Advanced Medical Technology, Ministry of Health, Labor and Welfare (H19-nano-010). The authors would like to express their deepest gratitude towards this grant. Authors would also like to express their gratitude for the help of Hokkaido Innovation through NanoTechnology Support (HINTS, Nanotechnology Network Project Supported by the Ministry of Education, Culture, Sports, Science and Technology).

REFERENCES

1. Suzuki, R., Oda, Y., Namai, E., Takizawa, T., Negishi, Y., Utoguchi, N., Tachibana, K., and Maruyama. K., Development of Site Specific Gene Delivery System with Sonoporation, *J. Pharm. Soc. Jpn.*, Vol. 128, No. 2, pp 187-192, 2008.
2. Maruyama, K., Suzuki, R., Takizawa, T., Utoguchi, N., and Negishi, Y., Drug and Gene Delivery by "Bubble Liposomes" and Ultrasound, *J. Pharm. Soc. Jpn.*, Vol. 127, No. 5, pp 781-787, 2007.
3. Hoff, L, Sontum, P. C., and Hovem, J. M., Oscillations of Polymeric Microbubbles: Effect of the Encapsulating Shell, *J. Acoust. Soc. Am.*, Vol. 107, No. 4, pp 2272-2280, 2000.

Int. J. Cancer: **122,** 2148–2153 (2008)

Synergistic antitumor activity of the novel SN-38-incorporating polymeric micelles, NK012, combined with 5-fluorouracil in a mouse model of colorectal cancer, as compared with that of irinotecan plus 5-fluorouracil

Takako Eguchi Nakajima[1,2], Masahiro Yasunaga[2], Yasuhiko Kano[3], Fumiaki Koizumi[4], Ken Kato[1], Tetsuya Hamaguchi[1], Yasuhide Yamada[1], Kuniaki Shirao[1], Yasuhiro Shimada[1] and Yasuhiro Matsumura[2]*

[1]*Gastrointestinal Oncology Division, National Cancer Center Hospital, Tokyo, Japan*
[2]*Investigative Treatment Division, Research Center for Innovative Oncology, National Cancer Center Hospital East, Kashiwa, Chiba, Japan*
[3]*Hematology Oncology, Tochigi Cancer Center, Tochigi, Japan*
[4]*Shien Lab Medical Oncology Division, National Cancer Center Hospital, Tokyo, Japan*

The authors reported in a previous study that NK012, a 7-ethyl-10-hydroxy-camptothecin (SN-38)-releasing nano-system, exhibited high antitumor activity against human colorectal cancer xenografts. This study was conducted to investigate the advantages of NK012 over irinotecan hydrochloride (CPT-11) administered in combination with 5-fluorouracil (5FU). The cytotoxic effects of NK012 or SN-38 (an active metabolite of CPT-11) administered in combination with 5FU was evaluated *in vitro* in the human colorectal cancer cell line HT-29 by the combination index method. The effects of the same drug combinations was also evaluated *in vivo* using mice bearing HT-29 and HCT-116 cells. All the drugs were administered i.v. 3 times a week; NK012 (10 mg/kg) or CPT11 (50 mg/kg) was given 24 hr before 5FU (50 mg/kg). Cell cycle analysis in the HT-29 tumors administered NK012 or CPT-11 *in vivo* was performed by flow cytometry. NK012 exerted more synergistic activity with 5FU compared to SN-38. The therapeutic effect of NK012/5FU was significantly superior to that of CPT-11/5FU against HT-29 tumors ($p = 0.0004$), whereas no significant difference in the antitumor effect against HCT-116 tumors was observed between the 2-drug combinations ($p = 0.2230$). Cell-cycle analysis showed that both NK012 and CPT-11 tend to cause accumulation of cells in the S phase, although this effect was more pronounced and maintained for a more prolonged period with NK012 than with CPT-11. Optimal therapeutic synergy was observed between NK012 and 5FU, therefore, this regimen is considered to hold promise of clinical benefit, especially for patients with colorectal cancer.

Key words: NK012; SN-38; 5-fluorouracil; drug delivery system; colorectal cancer

The 5-year survival rates of colorectal cancer (CRC) have improved remarkably over the last 10 years, accounted for in large part by the extensively investigated agents after 5-fluorouracil (5FU). Irinoetcan hydrochloride (CPT-11), a water-soluble, semi-synthetic derivative of camptothecin, is one such agent that has been shown to be highly effective, and currently represents a key-drug in first- and second-line treatment regimens for CRC. CPT-11 monotherapy, however, has not been shown to yield superior efficacy, including in terms of the median survival time, to bolus 5FU/leucovorin (LV) alone.[1] In 2 Phase III trials, the addition of CPT-11 to bolus or infusional 5FU/LV regimens clearly yielded greater efficacy than administration of 5FU/LV alone, with a doubling of the tumor response rate and prolongation of the median survival time by 2–3 months.[1,2]

CPT-11 is converted to 7-ethyl-10-hydroxy-camptothecin (SN-38), a biologically active and water-insoluble metabolite of CPT-11, by carboxylesterases in the liver and the tumor. SN-38 has been demonstrated to exhibit up to a 1,000-fold more potent cytotoxic activity than CPT-11 against various cancer cells *in vitro*.[3] The metabolic conversion rate is, however, very low, with only <10% of the original volume of CPT-11 being metabolized to SN-38[4,5]; conversion of CPT-11 to SN-38 also depends on genetic interindividual variability of the activity of carboxylesterases.[6] Direct use of SN-38 itself for clinical cancer treatment must be shown to be identical in terms of both efficacy and toxicity.

Some drugs incorporated in drug delivery systems (DDS), such as Abraxane and Doxil, are already in clinical use.[7,8] The clinical benefits of DDS are based on their EPR effect.[9] The EPR effect is based on the pathophysiological characteristics of solid tumor tissues: hypervascularity, incomplete vascular architecture, secretion of vascular permeability factors stimulating extravasation within cancer tissue, and absence of effective lymphatic drainage from the tumors that impedes the efficient clearance of macromolecules accumulated in solid tumor tissues. Several types of DDS can be used for incorporation of a drug. A liposome-based formulation of SN-38 (LE-SN38) has been developed, and a clinical trial to assess its efficacy is now under way.[10,11]

Recently, we demonstrated that NK012, novel SN-38-incorporating polymeric micelles, exerted superior antitumor activity and less toxicity than CPT-11.[12] NK012 is characterized by a smaller size of the particles than LE-SN38; the mean particle diameter of NK012 is 20 nm. NK012 can release SN-38 under neutral conditions even in the absence of a hydrolytic enzyme, because the bond between SN-38 and the block copolymer is a phenol ester bond, which is stable under acidic conditions and labile under mild alkaline conditions. The release rate of SN-38 from NK012 under physiological conditions is quite high; more than 70% of SN-38 is released within 48 hr. We speculated that the use of NK012, in place of CPT-11, in combination with 5FU may yield superior results in the treatment of CRC. In the present study, we evaluated the antitumor activity of NK012 administered in combination with 5FU as compared to that of CPT-11 administered in combination with 5FU against CRC in an experimental model.

Material and methods

Cells and animals

The human colorectal cancer cell lines used, namely, HT-29 and HCT-116, were purchased from the American Type Culture Collection (Rockville, MD). The HT-29 cells and HCT-116 cells were maintained in RPMI 1640 supplemented with 10% fetal bovine serum (Cell Culture Technologies, Gaggenau-Hoerden, Germany), penicillin, streptomycin, and amphotericin B (100 units/mL, 100 μg/mL, and 25 μg/mL, respectively; Sigma, St. Louis, MO) in a humidified atmosphere containing 5% CO_2 at 37°C.

BALB/c *nu/nu* mice were purchased from SLC Japan (Shizuoka, Japan). Six-week-old mice were subcutaneously (s.c.)

***Correspondence to:** Investigative Treatment Division, Research Center for Innovative Oncology, National Cancer Center Hospital East, 6-5-1 Kashiwanoha, Kashiwa, Chiba 277-8577, Japan. Fax: +81-4-7134-6866. E-mail: yhmatsum@east.ncc.go.jp
Received 2 September 2007; Accepted after revision 20 November 2007
DOI 10.1002/ijc.23381
Published online 14 January 2008 in Wiley InterScience (www.interscience.wiley.com).

inoculated with 1×10^6 cells of HT-29 or HCT-116 cell line in the flank region. The length (a) and width (b) of the tumor masses were measured twice a week, and the tumor volume (TV) was calculated as follows: $TV = (a \times b^2)/2$. All animal procedures were performed in compliance with the Guidelines for the Care and Use of Experimental Animals established by the Committee for Animal Experimentation of the National Cancer Center; these guidelines meet the ethical standards required by law and also comply with the guidelines for the use of experimental animals in Japan.

Drugs

The SN-38-incorporating polymeric micelles, NK012, and SN-38 were prepared by Nippon Kayaku (Tokyo, Japan).[12] CPT-11 was purchased from Yakult Honsha (Tokyo, Japan). 5FU was purchased from Kyowa Hakko (Tokyo, Japan).

Cell growth inhibition assay

HT-29 cells were seeded in 96-well plates at a density of 2,000 cells/well in a final volume of 90 μL. Twenty-four hours after seeding, a graded concentration of NK012 or SN-38 was added concurrently with 5FU to the culture medium of the HT-29 cells in a final volume of 100 μL for drug interaction studies. The culture was maintained in the CO_2 incubator for an additional 72 hr. Then, cell growth inhibition was measured by the tetrazolium salt-based proliferation assay (WST assay; Wako Chemicals, Osaka, Japan). WST-1 labeling solution (10 μL) was added to each well and the plates were incubated at 37°C for 3 hr. The absorbance of the formazan product formed was detected at 450 nm in a 96-well spectrophotometric plate reader. Cell viability was measured and compared to that of the control cells. Each experiment was carried out in triplicate and was repeated at least 3 times. Data were averaged and normalized against the nontreated controls to generate dose-response curves.

Drug interaction analysis

The nature of interaction between NK012 or SN-38 and 5FU against HT-29 cells was evaluated by median-effect plot analyses and the combination index (CI) method of Chou and Talalay.[13] Data analysis was performed using the Calcusyn software (Biosoft, NY, USA). NK012 or SN-38 was combined with 5FU at a fixed ratio that spanned the individual IC_{50} values of each drug. The IC_{50} values were determined on the basis of the dose-response curves using the WST assay. For any given drug combination, the CI is known to represent the degree of synergy, additivity or antagonism. It is expressed in terms of fraction-affected (*Fa*) values, which represents the percentage of cells killed or inhibited by the drug. Isobologram equations and *Fa*/CI plots were constructed by computer analysis of the data generated from the median effect analysis. Each experiment was performed in triplicate with 6 gradations and was repeated at least 3 times. The resultant dose-response curves were averaged, to create a single composite dose-response curve for each combination.

In vivo analysis of the effects of NK012 combined with 5FU as compared to those of CPT-11 combined with 5FU

When the mean tumor volumes reached ~93 mm^3, the mice were randomly divided into test groups consisting of 5 mice per group (Day 0). The drugs were administered i.v. *via* the tail vein of the mice. In the groups administered NK012 or 5FU as single agents, the drug was administered on Days 0, 7 and 14. In the combined treatment groups, NK012 or CPT-11 was administered 24 hr before 5FU on Days 0, 7 and 14, according to the previously reported combination schedule for CPT-11 and 5FU.[14] Complete response (CR) was defined as tumor not detectable by palpation at 90 days after the start of treatment, at which time-point the mice were sacrificed. Tumor volume and body weight were measured twice a week. As a general rule, animals in which the tumor volume exceeded 2,000 mm^3 were also sacrificed.

Experiment 1. Evaluation of the effects of NK012 combined with 5FU and determination of the maximum tolerated dose (MTD) of NK012/5FU. By comparing the data between NK012 administered as a single agent and NK012/5FU, we evaluated the effects of the combined regimen against the s.c HT-29 tumors. A preliminary experiment showed that combined administration of NK012 15 mg/kg + 5FU 50 mg/kg every 6 days caused drug-related lethality (data not shown). To determine the MTD, therefore, we set the dosing schedule of the combined regimen at 5 or 10 mg/kg of NK012 + 50 mg/kg of 5FU three times a week.

Experiment 2. Comparison of the antitumor effect of NK012/5FU and CPT-11/5FU. Based on a comparison of the data between NK012/5FU and CPT-11/5FU against the s.c. HT-29 and HCT-116 tumors, we investigated the feasibility of the clinical application of NK012/5FU for the treatment of CRC. CPT-11/5FU was administered three times a week at the respective MTDs of the 2 drugs as previously reported, that is, CPT11 at 50 mg/kg and 5FU at 50 mg/kg, respectively.[14] NK012/5FU was administered once three times a week at the respective MTDs of the 2 drugs determined from Experiment 1.

Cell cycle analysis

Samples from the HT-29 tumors that had grown to 80–100 mm^3 were removed from the mice at 6, 24, 48, 72 and 96 hr after the administration of NK012 alone at 10 mg/kg or CPT-11 alone at 50 mg/kg. The samples were excised, minced in PBS and fixed in 70% ethanol at −20°C for 48 hr. They were then digested with 0.04% pepsin (Sigma chemical Co., St Lous, MO) in 0.1 N HCL for 60 min at 37°C in a shaking bath to prepare single-nuclei suspensions. The nuclei were then centrifuged, washed twice with PBS and stained with 40 μg/mL of propidium iodide (Molecular Probes, OR) in the presence of 100 μg/mL RNase in 1 mL PBS for 30 min at 37°C. The stained nuclei were analyzed with B-D FACSCalibur (BD Biosciences, San Jose, CA), and the cell cycle distribution was analyzed using the Modfit program (Verity Software House Topsham, ME).

Statistical analyses

Data were expressed as mean ± SD. Data were analysed with Student's t test when the groups showed equal variances (F test), or Welch's test when they showed unequal variances (F test). $p < 0.05$ was regarded as statistically significant. All statistical tests were 2-sided.

Results

Antiproliferative effects of NK012 or SN-38 administered in combination with 5FU

Figure 1*a* shows the dose-response curves for NK012 alone, 5FU alone and a combination of the two. The IC_{50} levels of NK012 and 5FU against the HT-29 cells were 39 nM and 1 μM, respectively, and the IC_{50} level of SN-38 was 14 nM (data not shown). Based on these data, the molar ratio of NK012 or SN-38:5FU of 1:1,000 was used for the drug combination studies.

Figures 1*b* and 1*c* show the median-effect and the combination index plots. Combination indices (CIs) of <1.0 are indicative of synergistic interactions between 2 agents; additive interactions are indicated by CIs of 1.0, and antagonism by CIs of >1.0. Figure 1*c* shows the combination index for NK012 and 5FU, when 2 drugs are supposed to be mutually exclusive. Marked synergism was observed between Fa 0.2 and 0.6. Theoretically, the CI method is the most reliable around an Fa of 0.5, suggesting synergistic effects of the combination of NK012 and 5FU. This synergistic effect was more evident than that of SN-38/5FU (Fig. 1*d*).

In vivo *effect of combined NK012 and 5FU*

Experiment 1. Dose optimization and effect of combined NK012 and 5FU against HT-29 tumors. Comparison of the relative tumor volumes on Day 40 revealed significant differences between

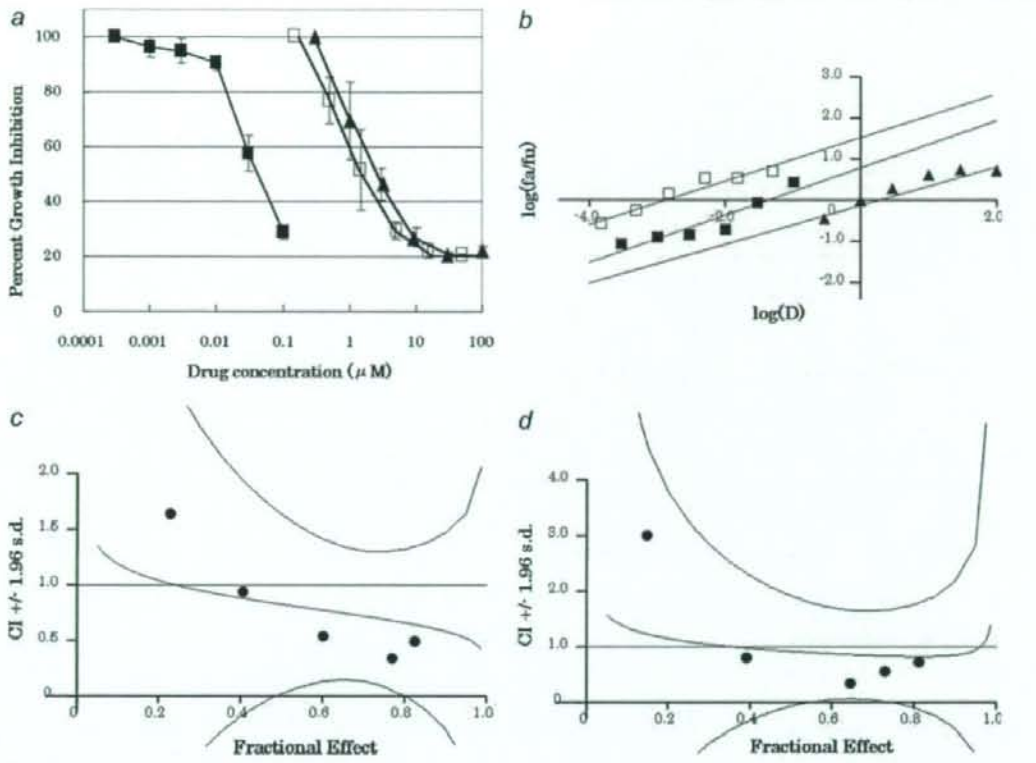

FIGURE 1 – Interaction of NK012 and 5FU *in vitro*. (*a*) Dose-response curves for NK012 alone (■), 5FU alone (▲) and their combination (□) against HT-29 cells. HT-29 cells were seeded at 2,000 cells/well. Twenty-four hours after seeding, a graded concentration of NK012 or 5FU was added to the culture medium of the HT-29 cells. Cell growth inhibition was measured by WST assay after 72 hr of treatment. Cell viability was measured and compared with that of the control cells. Each experiment was carried out independently and repeated at least 3 times. Points, mean of tripricates; bars, SD. (*b*) Median effect plot for the interaction of NK012 and 5FU. (*c*, *d*) Combination index for the interaction as a function of the level of effect (fraction effect = 0.5 is the IC_{50}). The straight line across the CI value of 1.0 indicates additive effect and CIs above and below indicate antagonism and synergism, respectively. The molar ratio of NK012/5FU (*c*) or SN-38/5FU (*d*) at 1:1,000 was tested by CI analysis. Black circles represent the CIs of the actual data points, solid lines represent the computer-derived CIs at effect levels ranging from 10 to 100% inhibition of cell growth, and the dotted lines represent the 95% confidence intervals.

those in the mice administered NK012 alone and those administered NK012/5FU at 5 mg/kg of NK012 ($p = 0.018$) (Fig. 2*a*). Although there was no statistically significant difference in the relative tumor volume measured on Day 54 between the mice administered NK012 alone and NK012/5FU at 10 mg/kg of NK012 ($p = 0.3050$), a trend of superior antitumor effect was demonstrated in the group treated with NK012/5FU at 10 mg/kg of NK012 (Fig. 2*a*). The CR rates were 20, 40 and 60% for 5 mg/kg NK012 + 50 mg/kg 5FU, 10 mg/kg NK012 alone and 10 mg/kg NK012 + 50 mg/kg 5FU, respectively. The schedule of 10 mg/kg NK012 + 50 mg/kg 5FU resulted in no remarkable toxicity in terms of body weight changes, and these doses were determined as representing the MTDs (Fig. 2*b*).

Experiment 2. Comparison of the antitumor effect of combined NK012/5FU and CPT-11/5FU against HT-29 and HCT-116 tumors. The therapeutic effect of NK012/5FU on Day 60 was significantly superior to that of CPT-11/5FU against the HT-29 tumors ($p = 0.0004$) (Fig. 3*a*). A more potent antitumor effect, namely, a 100% CR rate, was obtained in the NK012/5FU group as compared to the 0% CR rate in the CPT-11/5FU group. Although no statistically significant difference in the relative tumor volume on Day 61 was demonstrated between the NK012/5FU and CPT-11/5FU in the case of the HCT-116 tumors ($p = 0.2230$), a trend of superior antitumor effect against these tumors was observed in the NK012/5FU treatment group (Fig. 3*b*). The CR rates for the case of the HCT-116 tumors were 0% in both NK012/5FU and CPT-11/5FU groups.

Specificity of cell cycle perturbation

We studied the differences in the effects between NK012 10 mg/kg and CPT-11 50 mg/kg on the cell cycle (Fig. 4*a*). The data indicated that both NK012 and CPT-11 tended to cause accumulation of cells in the S phase, although the effect of NK012 was stronger and maintained for a more prolonged period than that of CPT-11; the maximal percentage of S-phase cells in the total cell population in the tumors was 34% at 24 hr after the administration of CPT-11, whereas it was 39% at 48 hr after the administration of NK012 (Figs. 4*b*, and 4*c*).

Discussion

Our primary endpoint was to clarify the advantages of NK012 over CPT-11 administered in combination with 5FU. We demonstrated that combined NK012 and 5FU chemotherapy exerts more